Changes in Quaternary Structure in the Signaling Mechanisms of PAS Domains[†,‡]

Rebecca A. Ayers and Keith Moffat*

Department of Biochemistry and Molecular Biology, The University of Chicago, 929 East 57th Street, Chicago, Illinois 60637

Received July 3, 2008; Revised Manuscript Received August 15, 2008

ABSTRACT: FixL from *Bradyrhizobium japonicum* is a PAS sensor protein in which two PAS domains covalently linked to a histidine kinase domain are responsible for regulating nitrogen fixation in an oxygen-dependent manner. The more C-terminal PAS domain, denoted *bj*FixLH, contains a heme cofactor that binds diatomic molecules such as carbon monoxide and oxygen and regulates the activity of the FixL histidine kinase as part of a two-component signaling system. We present the structures of ferric, deoxy, and carbon monoxide-bound *bj*FixLH in a new space group (*P*1) and at resolutions (1.5−1.8 Å) higher than the resolutions of those previously obtained. Interestingly, *bj*FixLH can form two different dimers (in *P*1 and *R*32 crystal forms) in the same crystallization solution, where the monomers in one dimer are rotated ∼175° relative to the second. This suggests that PAS monomers are plastic and that two quite distinct quaternary structures are closely similar in free energy. We use screw rotation analysis to carry out a quantitative pairwise comparison of PAS quaternary structures, which identifies five different relative orientations adopted by isolated PAS monomers. We conclude that PAS monomer arrangement is context-dependent and could differ depending on whether the PAS domains are isolated or are part of a full-length protein. Structurally homologous residues comprise a conserved dimer interface. Using network analysis, we find that the architecture of the PAS dimer interface is continuous rather than modular; the network of residues comprising the interface is strongly connected. A continuous dimer interface is consistent with the low dimer−monomer dissociation equilibrium constant. Finally, we quantitate quaternary structural changes induced by carbon monoxide binding to a *bj*FixLH dimer, in which monomers rotate by up to ∼2° relative to each other. We relate these changes to those in other dimeric PAS domains and discuss the role of quaternary structural changes in the signaling mechanisms of PAS sensor proteins.

The PAS[1] (Per-ARNT-Sim) superfamily is composed of sensor and polymerization domains that receive and transmit environmental signals to regulate cellular behavior (*1*). Signals include light, oxygen, and redox potential. PAS domains regulate many different types of effector domains such as kinases, phosphodiesterases, and transcription factors in a signal-dependent manner (*2*). The modular nature of proteins containing PAS or other signaling domains (*3*) enables signaling networks to be diverse and poses an interesting question: how can a single type of sensor domain with a largely conserved tertiary structure regulate effector domains with very diverse structures and functions? We address this question by examining signal recognition, initiation, and propagation in the PAS sensor domain.

Heme-PAS domains comprise a subset of the PAS superfamily distinguished by their iron protoporphyrin IX (heme b) cofactor, which binds oxygen and other diatomic molecules such as CO and nitric oxide (*4*). One example of a heme-PAS signaling protein is FixL, found in rhizobia and bacteria, which is responsible for regulating nitrogen fixation, anaerobic and microaerobic respiration, and hydrogen metabolism under hypoxic conditions (*3*). Rhizobial FixL proteins contain a histidine kinase effector domain, C-terminal to the heme-PAS domain, that is active and undergoes autophosphorylation in the absence of oxygen and is inactive in the presence of oxygen (*5*). The phosphate is transferred from FixL to FixJ, the response regulator in this two-component signaling system (*6*), and in a cascade of events leads to the upregulation of transcription from genes encoding proteins involved in nitrogen fixation (*5*−*7*). Regulation provides a safeguard against the prodigal use of energy to produce nitrogenase, an exquisitely oxygen sensitive protein, in the presence of oxygen.

Crystallographic studies of ligand-bound and ligand-free, deoxy (ferrous) forms of the heme-PAS domains of FixL proteins from *Bradyrhizobium japonicum* (*bj*FixLH) and *Sinorhizobium meliloti* (*sm*FixLH) and of the direct oxygen sensor from *Escherichia coli* (*ec*DOSH) have explored the mechanisms of signal recognition and initiation in heme-PAS domains (*8*−*12*). These structures suggest that ligand-dependent tertiary structural changes in FixLH are at least partly responsible for regulating effector domain activity. *bj*FixLH undergoes ligand-dependent conformational changes in the FG loop and the H_β and I_β strands. The movement in

[†] This work is supported by National Institutes of Health (NIH) Grant GM036452 to K.M. BioCARS is supported by NIH Grant RR07707 to K.M. Use of the Advanced Photon Source is supported by the U.S. Department of Energy, Office of Science, Office of Basic Energy Sciences, under Contract DE-AC02-06CH11357.

[‡] The structures have been deposited in the Protein Data Bank (PDB) as entries 2VV6, 2VV7, and 2VV8.

* To whom correspondence should be addressed. Phone: (773) 702-1801. Fax: (773) 702-0439. E-mail: moffat@cars.uchicago.edu.

[1] Abbreviations: PAS, Per-ARNT-Sim; CO, carbon monoxide; PEI, polyethylenimine; CAPSO, 3-(cyclohexylamino)-2-hydroxy-1-propanesulfonic acid.

10.1021/bi801254c CCC: $40.75
Published on Web 10/23/2008

the FG loop has been described as the "FG-loop switch" and may be important for the signal-dependent regulation of FixL kinase activity (*10*−*13*). Quaternary structural changes may also play a role. *bj*FixL forms a homodimer and in the absence of oxygen autophosphorylates at a histidine residue that is conserved among sensor histidine kinases (*6, 14, 15*). Key and colleagues suggested (*10*) that quaternary structural changes which reorient *bj*FixLH subunits relative to each other may facilitate *bj*FixL autophosphorylation. Quaternary structural changes may be a general mechanism by which PAS sensor proteins modulate the activity of their effector domains. For example, the blue light photosensor LOV domain of the dimeric PAS sensor protein, YtvA, in *Bacillus subtilis* (*bs*YtvA-LOV) undergoes small but significant quaternary structural changes as a result of light absorption (*16*).

Here we report the structures of met (ferric), deoxy, and CO-bound forms of *bj*FixLH in a new space group, *P*1, and at a resolution (1.5−1.8 Å) higher than that previously obtained (1.8−2.0 Å) (*10*). Four *bj*FixLH monomers in the unit cell are arranged as two dimers related by noncrystallographic 2-fold symmetry. Since packing of protein molecules in the crystal lattice can influence conformational changes (*17*), we compare *bj*FixLH structures and signal-dependent conformational changes in the *P*1 space group with those previously observed in the *C*2 and *R*32 space groups (*10*). We quantitate the differences in quaternary structure of *bj*FixLH in the different space groups (P1AB, P1CD, C2AB, and R32) and compare the quaternary structures of *bj*FixLH to those of other PAS dimers, using screw rotation analysis. To characterize the architecture of the PAS dimer interface, we carry out network analysis on contact maps describing the interactions among dimer interface residues. Screw rotation and network analyses identify how PAS monomers pack together to form dimers, and the continuous or modular nature of the dimer interface.

MATERIALS AND METHODS

*Expression and Crystallization. bj*FixLH (residues 140−280) was purified as described previously (*10, 18*). Crystals were grown in the oxidized, met form using the hanging drop vapor diffusion method with 3.75 M NaCl, 1.5% PEI, and 50 mM CAPSO (pH 9) at a protein concentration of 60 mg/mL. Deoxy-*bj*FixLH and CO-*bj*FixLH crystals were made as previously described (*10*) by reducing the met form with mother liquor containing 200 mM ascorbate and then gently bubbling in either nitrogen or CO for 1 or 2 h, respectively. All crystals were cryocooled by being plunged into liquid nitrogen (100 K). No additional cryoprotectants were found to be necessary.

Data Collection, Reduction, and Refinement. Monochromatic X-ray oscillation data were collected at 100 K at the BioCARS 14 BM-C beamline at the Advanced Photon Source (Argonne National Laboratory, Argonne, IL). Data indexing, scaling, and integration were conducted using HKL2000 (*19*). Molecular replacement was conducted using EPMR (*20*) with the deoxy-*bj*FixLH [Protein Data Bank (PDB) entry 1XJ3] structure as a search model (*10*). Rigid body refinement, simulated annealing refinement, individual isotropic *B*-factor refinement, and conjugate-gradient minimization were performed using CNS (*21*) and REFMAC (*22*). Model building was conducted using X-fit/Xtalview (*23*) and Coot (*24*). Figures were created using MOLMOL (*25*), Pymol (*26*), and MegaPov.

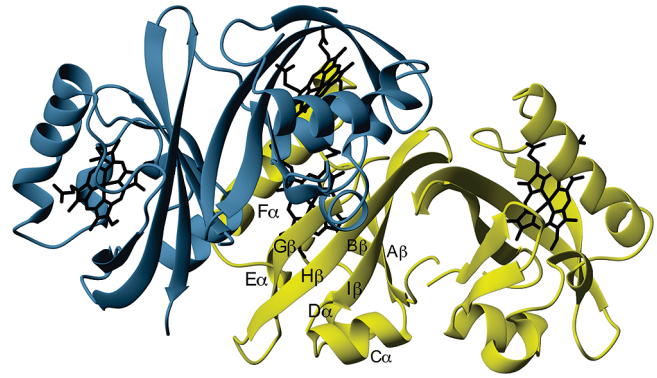

FIGURE 1: Ribbon diagram of the structure of deoxy *bj*FixLH in the *P*1 crystal form. P1AB and P1CD dimers are colored yellow and blue, respectively. Secondary structure elements are labeled on the P1B monomer.

Structure Analysis. The buried surface area and theoretical free energy of solvation were calculated using PISA (*27*). The number of inter- and intrachain contacts was calculated using the CCP4 program NCONT (*28*) with a cutoff value of <5 Å between two atoms of interacting residues. The specificity and chemical nature of these interactions were determined using Contacts of Structural Units (CSU) (*29*) and visualized using Pajek (*30*). To identify main chain tertiary structural differences, we superimposed individual monomers using Cα least-squares fit analysis and then calculated the root-mean-square deviation (rmsd) of Cα atoms (*31, 32*). Quaternary structural changes were determined using rigid-body screw rotation analysis, which can be described as a "fit−refit" method (*32*−*35*). Two monomers from the pair of dimers being compared were superimposed using Cα least-squares fit analysis. The screw rotation parameters were then obtained, namely, the magnitude of rotation (ρ) and translation (d) associated with a second (rigid body) superposition between the previously nonsuperimposed monomers. Superposition and calculation of rotation and translation parameters were carried out using the CCP4 program LSQKAB (*28, 36*).

RESULTS

Structure of bjFixLH in the P1 Space Group at 1.5−*1.8 Å Resolution.* The structures of *bj*FixLH in the deoxy (ferrous, Fe^{2+}), met (ferric, Fe^{3+}), and CO-bound states were determined in the *P*1 crystal form at resolutions ranging from 1.5 to 1.8 Å (Figure 1). CO was used instead of oxygen, the physiological ligand of *bj*FixL, to study signal-induced conformational changes in three crystal forms (*P*1, *C*2, and *R*32) of *bj*FixLH. At present, only one crystal form of oxygen-bound *bj*FixLH has been determined (*13*). Both oxygen and CO form low-spin complexes with the ferrous heme in *bj*FixLH and inhibit *bj*FixL autophosphorylation (*37*). Oxygen and CO binding also elicit largely similar tertiary conformational changes in *bj*FixLH, which suggests that oxygen and CO share a common signaling mechanism (*10*). Data collection and refinement statistics are presented in Table 1. Electron density could be identified and fitted for residues 154−257 in all four monomers (A, B, C, and

Table 1: Data Collection and Refinement Statistics for *bj*FixLH in Space Group *P*1

	met	deoxy	CO
Diffraction Data			
unit cell dimensions			
a, *b*, *c* (Å)	48.8, 50.0, 59.0	48.6, 49.8, 58.8	48.9, 50.3, 59.0
α, *β*, *γ* (deg)	73.7, 70.4, 72.3	73.2, 71.1, 71.7	73.4, 70.3, 72.1
resolution (Å) (last shell)	50.0−1.40 (1.45−1.40)	50.0−1.80 (1.86−1.80)	50.0−1.61 (1.67−1.61)
no. of unique reflections	91144	44159	57814
R_{merge} (%) (last shell)	3.4 (42.3)	4.6 (42.4)	3.5 (32.4)
redundancy (last shell)	1.9 (1.9)	3.8 (3.7)	1.9 (1.8)
completeness (%) (last shell)	94.6 (94.5)	96.1 (95.7)	90.7 (93.7)
$I/\sigma I$ (last shell)	25.3 (2.1)	38.0 (3.2)	29.5 (3.7)
Refinement			
resolution (Å)	44.7−1.50	46.3−1.81	46.9−1.61
R_{work}, R_{free} (%)	18.2, 21.1	19.7, 24.7	20.6, 24.9
rmsd for ideal bond lengths (Å)	0.010	0.019	0.015
rmsd for ideal bond angles (deg)	1.435	1.985	1.643
Ramachandran Distribution			
most favored (%)	92.5	91.1	91.4
allowed (%)	7.5	8.9	8.6
generously allowed (%)	0	0	0
disallowed (%)	0	0	0
PDB entry	2VV6	2VV7	2VV8

D) in the unit cell in each state, but not for the 11 N-terminal residues or for C-terminal residues 258−268, which form an α-helix in the *R*32 crystal form (*10*). All tertiary structures are closely similar (rmsd < 1.0 Å) to those found in other crystal forms and in other PAS domains. The four monomers are found as two dimers, P1AB and P1CD, related by a 2-fold noncrystallographic symmetry axis. When either P1AB or P1CD is superimposed on the C2 dimer (C2AB), the two nonsuperimposed dimers are rotated and displaced relative to each other. This reflects the different crystal packing arrangement in *P*1 compared to *C*2.

Comparison of PAS Domain Quaternary Structures. *bj*FixLH dimer formation in the crystal may reflect the dimeric nature of the full-length *bj*FixL sensor protein in solution (*18*). However, it is not known how PAS domains arrange themselves relative to each other within a signaling complex or what role quaternary structural changes play (if any) in the signaling mechanism of PAS sensor proteins. To address the first, we compared the dimeric structures of *bj*FixLH in three different crystal forms (*P*1, *C*2, and *R*32). *bj*FixLH forms noncrystallographic dimers in the *P*1 (P1AB and P1CD) and *C*2 (C2AB) crystal forms and a crystallographic dimer in the *R*32 crystal form.

The arrangement of monomers within a complex can be characterized by the position and type of residues comprising the interface, the buried surface area and/or the number of contacts made by interface residues, and by screw rotation parameters that describe any differences in quaternary structure. Each monomer in the *P*1 crystal form of *bj*FixLH contacts six neighbors and generates six candidate intra- and interunit cell dimeric assemblies. To assess which of the possible dimers is most stable and potentially physiologically relevant, we calculated the buried surface area and theoretical stability of all six (*27*). Only two dimers (P1AB and P1CD) contain more than 900 Å^2 of buried surface area (BSA) and have a theoretical solvation free energy for forming the dimer interface lower than −8 kcal/mol, benchmarks for physiologically relevant assemblies (*38, 39*). These two intraunit cell dimers are shown in Figure 1. The buried surface area in P1AB and P1CD is approximately 1600 Å^2, which is similar to that in the *C*2 (1400 Å^2) noncrystallographic and *R*32 (1200 Å^2) crystallographic dimers. In both P1AB and P1CD, the dimer interface is comprised of a central hydrophobic patch and flanking hydrogen bonding regions largely contributed by residues in the G_β, H_β, and I_β strands.

Table 2: Quaternary Structure of *bj*FixLH Dimers in Different Crystal Forms[a]

dimer 1	dimer 2	*ρ*	*d*
P1AB (1)	P1AB (2)	0.2	0.0
P1AB (1)	P1CD (1)	3.5	0.3
P1AB (1)	P1CD (2)	2.9	0.4
P1AB (1)	C2AB	2.4	0.1
P1AB (1)	R32	174.9	1.1
P1AB (2)	P1CD (1)	3.4	0.1
P1AB (2)	P1CD (2)	2.7	0.2
P1AB (2)	C2AB	2.4	0.2
P1AB (2)	R32	175.1	1.0
P1CD (1)	P1CD (2)	0.7	0.1
P1CD (1)	C2AB	2.3	0.2
P1CD (1)	R32	178.1	0.7
P1CD (2)	C2AB	2.1	0.1
P1CD (2)	R32	177.7	0.7
C2AB	R32	174.9	1.1

[a] The monomer orientation of *bj*FixLH dimers in the deoxy state was compared using screw rotation analysis. Screw rotation parameters [rotation (*ρ*) in degrees and translation (*d*) in angstroms] are given for each pairwise comparison of dimers (dimer 1 and dimer 2). Data for two separate crystals (denoted 1 and 2) of deoxy *bj*FixLH in the *P*1 crystal form are listed.

We quantitated the differences in quaternary structure using screw rotation angle (*ρ*) and translation (*d*) parameters (Table 2). When one monomer from each of the *P*1 and *C*2 dimers is superimposed (rmsd ∼ 0.5 Å), the second (nonsuperimposed) monomer exhibits a small screw rotation of up to 3.5° and a translation of less than 1 Å. In contrast, a large screw rotation of ∼175° is observed when a monomer from either the *P*1 or *C*2 dimer is compared with a monomer in the *R*32 form. The ability of *bj*FixLH to adopt two different quaternary structures (in the *P*1 and *R*32 crystal forms) in the same solvent reflects the plasticity of PAS

Table 3: Quaternary Structures of PAS Domain Dimers Fall into Five Distinct Groups[a]

dimer 1	dimer 2	ρ	d	mean ρ, d ($\pm$standard deviation)
P1AB	R32	174.9	1.1	168.8 ± 7.7, 5.4 ± 4.2
P1AB	*sm*FixLH[b]	170.0	8.1	
P1AB	*ec*DOSH[b]	161.0	7.7	
P1AB	*av*NifL[b]	177.4	9.5	
*bs*YtvA-LOV	*cr*Phot-LOV1	160.9	0.7	
P1AB	*bs*YtvA-LOV	142.9	1.1	136.4 ± 7.5, 6.6 ± 5.6
R32	*cr*Phot-LOV1	134.7	0.0	
*sm*FixLH[b]	*cr*Phot-LOV1	130.2	10.1	
*cr*Phot-LOV1	*ec*DOSH[b]	128.7	9.5	
*cr*Phot-LOV1	*av*NifL[b]	145.4	12.3	
*ec*DOSH[b]	R32	75.8	3.7	76.4 ± 0.8, 2.1 ± 2.3
R32	*av*NifL[b]	76.9	12.9	
*ec*DOSH[b]	*bs*YtvA-LOV	65.4	4.5	
P1AB	*cr*Phot-LOV1	57.8	3.6	54.8 ± 7.9, 3.3 ± 1.3
R32	*bs*YtvA-LOV	46.5	2.9	
R32	*sm*FixLH[b]	61.5	2.0	
*bs*YtvA-LOV	*sm*FixLH[b]	46.9	0.5	
*bs*YtvA-LOV	*av*NifL[b]	50.7	1.6	
*sm*FixLH[b]	*ec*DOSH[b]	11.4	0.9	16.7 ± 4.6, 1.6 ± 0.8
*sm*FixLH[b]	*av*NifL[b]	19.7	1.5	
*ec*DOSH[b]	*av*NifL[b]	19.0	2.4	

[a] The monomer orientation of PAS domain dimers was compared using screw rotation analysis. Screw rotation parameters [rotation (ρ) in degrees and translation (d) in angstroms] are given for each pairwise comparison of dimers (dimer 1 and dimer 2). Only P1AB and R32 crystal forms of *bj*FixLH are shown since P1AB, P1CD, and C2AB have very similar quaternary structures ($\rho = 2.8 \pm 0.6°$; $d = 0.2 \pm 0.1$ Å). The mean rotation and translation parameters are listed for the five different PAS domain orientations identified using hierarchical clustering analysis. [b] PAS domains that contain ordered N-terminal helices.

domains, namely their ability to arrange themselves in different ways within a complex.

Do these observations of different quaternary structures in *bj*FixLH extend to other PAS domains that form dimers? To address this question, we compared the dimers of *bj*FixLH (in the *P*1, *C*2, and *R*32 space groups) (*10*), YtvA-LOV from *B. subtilis* (*bs*YtvA-LOV) (*16*), DOSH from *E. coli* (*ec*DOSH) (*8*), NifL from *Azotobacter vinelandii* (*av*NifL) (*40*), FixLH from *S. meliloti* (*sm*FixLH) (*9*), and LOV1 from *Chlamydomonas reinhardtii* (*cr*Phot-LOV1) (*41*) according to their screw rotation parameters. The last two molecules each form crystallographic dimers. Each physiologically relevant dimer was identified using the same criteria used to identify dimers of *bj*FixLH. Five distinct monomer orientations (Table 3) were identified by carrying out hierarchical clustering analysis on the pairwise comparisons of PAS dimer quaternary structure. Qualitative differences in PAS quaternary structure are presented in Figure 2, in which the left monomers are superimposed by a rigid body Cα least-squares fit superposition to chain B in P1AB and the right monomers display a range of orientations. Several interesting results are evident from Table 3. Structures containing ordered N-terminal helices (*sm*FixLH, *ec*DOSH, and *av*NifL) exhibit similar quaternary structures ($\rho = 16.7 \pm 4.6°$) and a small translation ($d = 1.6 \pm 0.8$ Å). Structures lacking an ordered N-terminal helix (*bj*FixLH, *bs*YtvA LOV, and *cr*Phot-LOV1) exhibit three distinct quaternary structures ($\rho \sim 50°$, 140°, and 170°) accompanied by a similarly small translation ($d = 1.6 \pm 1.4$ Å). This is opposed to when a structure containing an ordered N-terminal helix is compared to one lacking this helix, where a large translational component (range of 0.5−12.3 Å, with a mean of 6.2 ± 3.8 Å) is observed. The identification of only five distinct monomer orientations is surprising given that 21 pairwise comparisons were carried out in evaluating the quaternary structure of seven PAS dimers. The sources of constraints on monomer orientation are discussed below.

Conserved PAS Dimer Interface. Those residues in the P1AB, P1CD, C2, and R32 dimers that have more than 50% of their surface area buried at the dimer interface are indicated in the sequence alignment of PAS domains in Figure 3. From the alignment, it is apparent that homologous residues in *bj*FixLH, *sm*FixLH, ecDOSH, *bs*YtvA-LOV, *av*NifL, and *cr*Phot-LOV1 form the dimer interface in each protein despite in some cases very different quaternary structures. All are located on β-strands. Thus, a conserved set of residues forms the PAS domain intradimer interface regardless of crystal form, quaternary structure, or type of PAS domain. This is consistent with the observation by Erbel and colleagues (*42*) that the β-sheet is important for intra- and intermolecular interactions and versatile in its ability to accommodate both homo- and heterodimerization among PAS monomers (*42*).

To visualize the three-dimensional relationship among interface residues and the degree to which each residue contributes to the dimer interface, we determined the number of intra- and interunit cell crystal contacts made by each residue in the *P*1, *C*2, and *R*32 forms of *bj*FixLH, *sm*FixLH, *ec*DOSH, *bs*YtvA, *av*NifL, and *cr*Phot-LOV1 and mapped these contacts onto their tertiary structures (Figure 2). The conserved dimer interface residues are labeled in each structure.

Continuous or Modular Dimer Interface? Is the network of residues comprising the PAS dimer interface continuous, or can it be partitioned into clusters of residues, as described by Reichmann and colleagues (*43*) for proteins such as CheY/CheA and barnase/barstar? Clusters may contain as few as three residues. The boundaries between clusters are identified on the basis of the premise that residues within a cluster form many close connections (hydrophobic, aromatic, electrostatic, and hydrogen bonding) whereas relatively fewer connections are made between residues from different clusters (*43*).

To determine whether a PAS dimer interface is continuous or modular with at least two clusters, we created contact maps (Figure 4; see Materials and Methods) for P1AB, P1CD, C2AB, and R32 dimers containing those interface residues with >50% buried surface area at the dimer interface. Only specific interactions between two side chains or a side chain and main chain with contact atom distances of ≤5 Å were included. Nodes represent residues, and edges represent interactions between residues. The results of a hierarchical clustering analysis of each contact map revealed that the *bj*FixLH dimer interface contains only one large cluster, i.e., a continuous patch at the dimer interface. This result was maintained when the threshold for the distance between interacting atoms was lowered from 5 to 3.5 Å.

We extended this analysis to *sm*FixLH, *ec*DOSH, *bs*YtvA-LOV, *av*NifL, and *cr*Phot-LOV1 and observe the same result: in all molecules the PAS dimer interface contains a continuous patch. A large, well-developed cluster has been correlated with tight binding between monomers (*43*). The high affinity between PAS monomers (for example, K_d < 500 nM for *bs*YtvA-LOV) (*16*) is consistent with the

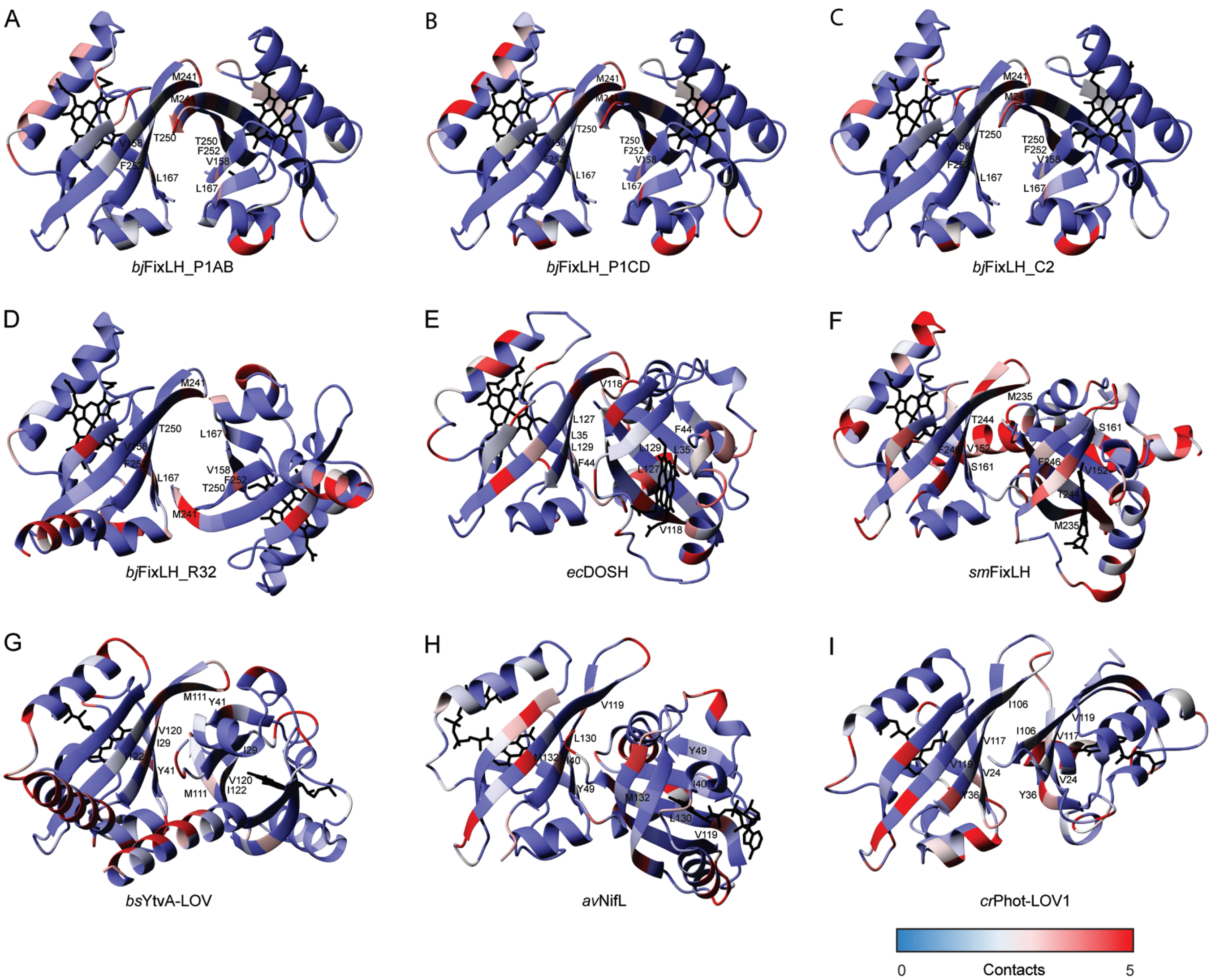

FIGURE 2: Intra- and interunit cell contacts between PAS monomers. The number of contacts made by residues in each monomer of (A) P1AB, (B) P1CD, (C) C2AB, (D) R32, (E) *ec*DOSH, (F) *sm*FixLH, (G) *bs*YtvA-LOV, (H) *av*NifL, and (I) *cr*Phot-LOV1 are colored according to the color scale bar. Conserved dimer interface residues are labeled by residue type and number.

```
                                               A'α      Aβ        Bβ   Cα    Dα    Eα         Fα                Gβ           Hβ          Iβ
bjFixLH_P1AB_A 151  ------------------------TIPDAMIVIDG---HGIIQLFSTAAERLFGWSELEAIGQNVNILMPEPDRSRHDSYISRYRTTSDPHIIGIGRIVTGKRRDGTTFPMHLSIGEMQSG-G-EPYFTGFVRD 255
bjFixLH_P1AB_B 151  ------------------------TIPDAMIVIDG---HGIIQLFSTAAERLFGWSELEAIGQNVNILMPEPDRSRHDSYISRYRTTSDPHIIGIGRIVTGKRRDGTTFPMHLSIGEMQSG-G-EPYFTGFVRD 255
bjFixLH_P1CD_C 151  ------------------------TIPDAMIVIDG---HGIIQLFSTAAERLFGWSELEAIGQNVNILMPEPDRSRHDSYISRYRTTSDPHIIGIGRIVTGKRRDGTTFPMHLSIGEMQSG-G-EPYFTGFVRD 255
bjFixLH_P1CD_D 151  ------------------------TIPDAMIVIDG---HGIIQLFSTAAERLFGWSELEAIGQNVNILMPEPDRSRHDSYISRYRTTSDPHIIGIGRIVTGKRRDGTTFPMHLSIGEMQSG-G-EPYFTGFVRD 255
bjFixLH_C2_A   151  ------------------------TIPDAMIVIDG---HGIIQLFSTAAERLFGWSELEAIGQNVNILMPEPDRSRHDSYISRYRTTSDPHIIGIGRIVTGKRRDGTTFPMHLSIGEMQSG-G-EPYFTGFVRD 255
bjFixLH_C2_B   151  ------------------------TIPDAMIVIDG---HGIIQLFSTAAERLFGWSELEAIGQNVNILMPEPDRSRHDSYISRYRTTSDPHIIGIGRIVTGKRRDGTTFPMHLSIGEMQSG-G-EPYFTGFVRD 255
bjFixLH_R32    151  ------------------------TIPDAMIVIDG---HGIIQLFSTAAERLFGWSELEAIGQNVNILMPEPDRSRHDSYISRYRTTSDPHIIGIGRIVTGKRRDGTTFPMHLSIGEMQSG-G-EPYFTGFVRD 255
smFixLH        122  GSHMLETEDVVRARDAHLRSILDTVPDATVVSAT---DGTIVSFNAAAVRQFGYAEEEVIGQNLRILMPEPYRHEHDGYLQRYMATGEKRIIGIDRVVSGQRKDGSTFPMKLAVGEMRSG-G-ERFFTGFIRD 249
ecDOSH_A         9  ----MKLTDADNAADGIFFPALEQNMMGAVLINE---NDEVMFFNPAAEKLWGYKREEVIGNNIDMLIPRDLRPAHPEYIRHNREGGKARVEGMSRELQLEKKDGSKIWTRFALSKVSA-EG-KVYYLALVRD 132
ecDOSH_B         9  ----MKLTDADNAADGIFFPALEQNMMGAVLINE---NDEVMFFNPAAEKLWGYKREEVIGNNIDMLIPRDLRPAHPEYIRHNREGGKARVEGMSRELQLEKKDGSKIWTRFALSKVSA-EG-KVYYLALVRD 132
bsYtvA-LOV_A    16  -----------------GSHMLDHVRVGVVITDPALEDNPIVYVNQGFVQMTGYETEEILGKNCRFLQGKHTDPAEVDNIRTALQNKEP----VTVQIQNYKKDGTMFWNELNIDPMEIED--KTYFVGIQND 125
bsYtvA-LOV_B    16  -----------------GSHMLDHVRVGVVITDPALEDNPIVYVNQGFVQMTGYETEEILGKNCRFLQGKHTDPAEVDNIRTALQNKEP----VTVQIQNYKKDGTMFWNELNIDPMEIED--KTYFVGIQND 125
avNifL_A        21  -----------ELLPEIFRQTVEHAPIAISITDL---KANILYANRAFRTITGYGSEEVLGKNESILSNGTTPRLVYQALWGRLAQKKP----WSGVLVNRRKDKTLYLAELTVAPVLNEAGETIYYLGMHRD 135
avNifL_B        21  -----------ELLPEIFRQTVEHAPIAISITDL---KANILYANRAFRTITGYGSEEVLGKNESILSNGTTPRLVYQALWGRLAQKKP----WSGVLVNRRKDKTLYLAELTVAPVLNEAGETIYYLGMHRD 135
crPhot-LOV1     17  ------------------------GLRHTFVVADATLPDCPLVYASEGFYAMTGYGPDEVLGHNCRFLQGEGTDPKEVQKIRDAIKKGEA----CSVRLLNYRKDGTPFWNLLTVTPIKTPDGRVSKFVGVQVD 122
                                                  *         *                                                                      *     * *
```

FIGURE 3: Structure-based sequence alignment of PAS domains. PAS sensor domain sequences were aligned using Dali (*59*) and then manually adjusted to best align secondary structure elements. Residues that have greater than 50% of their surface area buried (as calculated using PISA) at the dimer interface are colored red. Residues in italics are those for which the structure is unknown. Purple bars and asterisks indicate residues in the conserved dimer interface. Noncrystallographic dimers: *bj*FixLH (P1AB, P1CD, and C2), *ec*DOSH, *bs*YtvA-LOV, and *av*NifL. Crystallographic dimers: *bj*FixLH (R32), *sm*FixLH, and *cr*Phot-LOV1.

observation that PAS domain interfaces are comprised of a complex and continuous network of residues.

Effect of Quaternary Structure on Signal-Induced Tertiary Structural Changes. The observation that *bj*FixLH can adopt two distinct quaternary structures (*P*1 and *R*32) in the same crystallization solution raises an important question: To what extent do very different quaternary structures modify the signal-induced tertiary structural changes? CO-induced tertiary structural changes have been well-characterized in the *C*2 and *R*32 crystal forms (*10, 44*). Inspection of difference Fourier maps and calculation of Cα rmsd values for superimposed monomers (in the deoxy and CO-bound states) in the *P*1 and *R*32 crystal forms indicate that *bj*FixLH undergoes largely similar CO-induced tertiary structural changes regardless of its quaternary structure (with the exception of the dimer interface residue Thr250 discussed

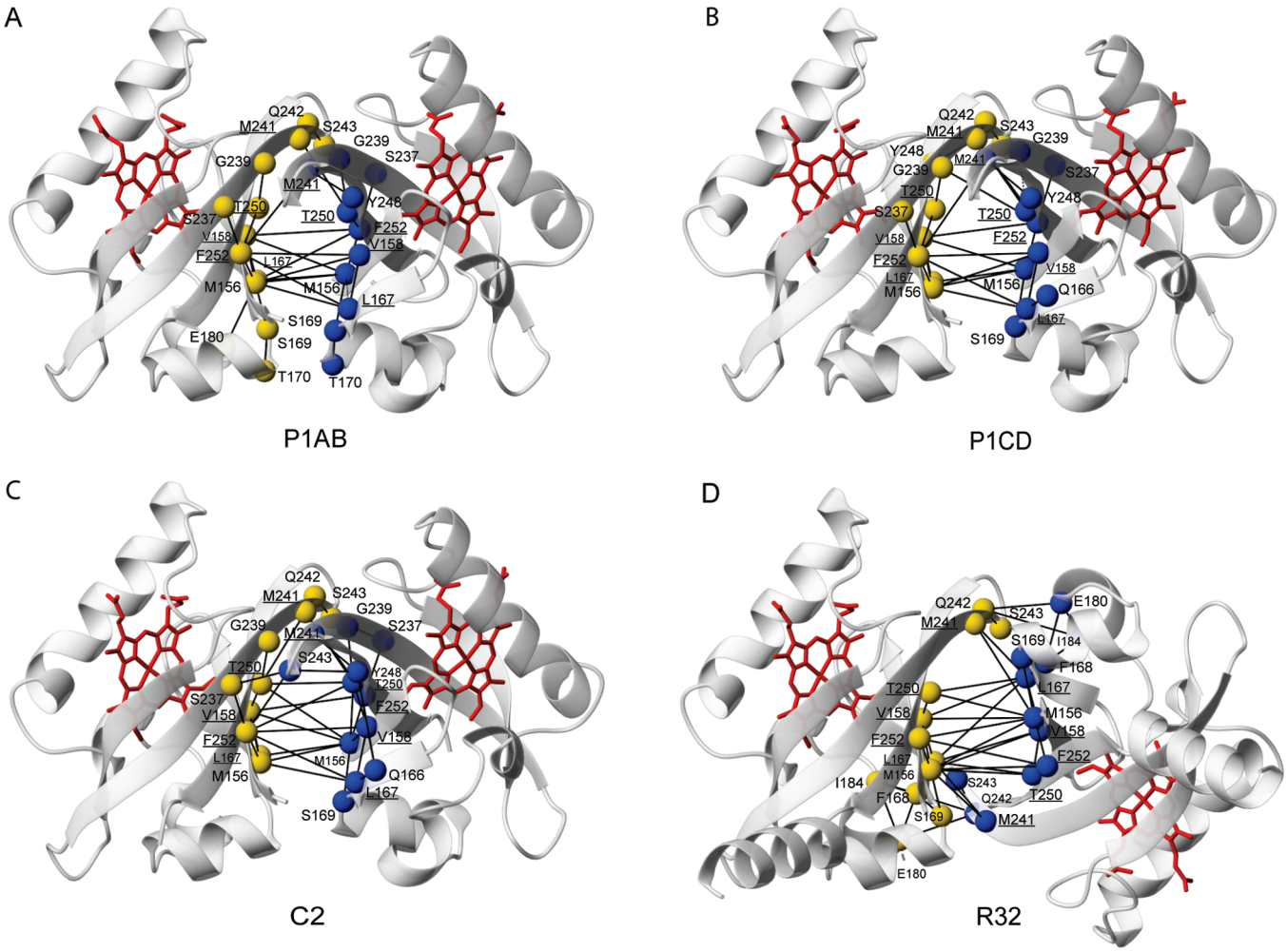

FIGURE 4: Contact map for the intradimer interface of *bj*FixLH dimers. The Cα atoms for residues making specific contacts with residues within the same or neighboring monomer were mapped onto their respective ribbon structures and are shown as spheres. Cα atoms from chain A of P1AB, C2AB, and R32 and from chain C of P1CD are shown as blue spheres. Cα atoms from chain B of P1A and B, C2AB, and R32 and from chain D of P1CD are shown as yellow spheres. Contacts are shown between two side chain atoms (solid line), between a side chain atom and a main chain atom (dotted line). Conserved dimer interface residues are underlined.

below). In both the *P*1 and *R*32 forms, very few tertiary structural changes are observed for main chain atoms. The largest tertiary structural changes occur in the side chains of residues known as the hydrophobic triad (I215, L236, and I238) that surround the heme active site, and residues located in the β-sheet on the distal side of the heme and the FG loop. The conformational changes in P1AB are similar in pattern but smaller in magnitude than those observed in P1CD. Most of these conformational changes are also observed for the third crystal form of *bj*FixLH, *C*2, despite quite different crystallization conditions (*10*).

Thr250 undergoes CO-induced conformational changes in dimers in the *P*1 crystal form but not in the *C*2 or *R*32 crystal form. We attribute this difference between crystal forms to different contacts made between Thr250 and other dimer interface residues (Figure 4). A second water molecule is also incorporated into the dimer interface in both P1AB and P1CD upon CO binding. The additional water molecule makes hydrogen bonds to the main chain amide and the side chain hydroxyl group of Thr250 in chain B of the P1AB dimer and Thr250 in chain C of the P1CD dimer. Conformational changes by Thr250 do not appear to be necessary for evoking CO-induced quaternary structural changes since *R*32 monomers rotate 1.5° relative to each other upon CO binding to the heme in the absence of tertiary structural changes at Thr250.

Signal-Induced Quaternary Structural Changes. To determine quaternary structural changes associated with ligand binding, we compared the structures of each dimer (P1AB and P1CD) in the *P*1 space group from two crystals, one in the CO-bound state and the other in the deoxy state. To provide a negative control, we also compared the structures of the P1AB and P1CD dimers derived from two deoxy crystals from which diffraction data were independently collected and refined to yield two deoxy structures. The magnitudes of subunit rotation and translation in P1AB and P1CD dimers following CO binding are compared in Table 4 with those for *bs*YtvA-LOV. In the negative control, monomers apparently rotate less than 0.7°, but monomers in the P1AB and P1CD dimers rotate by up to 1.3° and 1.9°, respectively. A similar rotation was observed in the *R*32 form (1.5°), but not in the *C*2 form, perhaps due to differences in crystallization solvent, crystal contacts, and interactions at the dimer interface. Signal-induced quaternary structural changes were also observed in the PAS domain dimer, *bs*YtvA, whose monomers rotate 2.2° after being exposed to light (*16*). Although similar in their magnitude of quaternary structural change, the different monomer arrange-

Table 4: Signal-Induced Quaternary Structural Changes by PAS Domains[a]

dimer 1	dimer 2	ρ	d
P1AB (deoxy)	P1AB (CO)	1.3	0.1
P1CD (deoxy)	P1CD (CO)	1.9	0.0
C2AB (deoxy)	C2AB (CO)	0.7	0.0
R32 (deoxy)	R32 (CO)	1.5	0.2
*bs*YtvA-LOV (dark)	*bs*YtvA-LOV (light)	2.2	0.1

[a] The monomer orientations of *bj*FixLH (in deoxy and CO-bound states) and *bs*YtvA-LOV (in dark and light states) were compared using screw rotation analysis. Screw rotation parameters [rotation (ρ) in degrees and translation (d) in angstroms] are given for each pairwise comparison of dimers (dimer 1 and dimer 2).

ments in *bj*FixLH and *bs*YtvA-LOV suggest that there are several ways in which PAS dimers could undergo quaternary structural changes as a result of responding to a signal.

DISCUSSION

PAS Domain Quaternary Structure. The quaternary structures of several PAS domain dimers have previously been determined (*8*−*10, 16, 40, 41*). By quantitating differences in PAS quaternary structure using screw rotation analysis, we identify five discrete monomer orientations (Table 3) that are adopted by PAS domains. Most strikingly, the presence of ordered N-terminal helices seems to predispose a dimer to a particular orientation in which the monomers adopt a parallel arrangement. Different monomer orientations may arise from differences in crystallization conditions. However, recent studies suggest that the N-terminal flanking region (termed the Ncap) stabilizes PAS dimers (*9, 45*−*47*). The signal transduction histidine kinase (STHK) H-NOXA from *Nostoc punctiforme* (*np*STHK H-NOXA), which has a PAS-like core fold, undergoes a change in monomer orientation as a result of deletion of seven N-terminal residues flanking its core (*48*). In this case, the N-terminal helices appear to be critical for maintaining a parallel orientation. Deletion of the N-terminal flanking region of a PAS domain from *Rhodobacter sphaeroides* PpsR, a transcription factor, disrupts its repressor activity but not its oligomerization state (*49*). Together, these data suggest that the Ncap may be of general importance in establishing the quaternary structure and function of PAS domains.

The presence of N-terminal domains and, in particular, dimerization domains may also affect the arrangement of PAS domains in PAS sensor proteins. Recently, the dimeric structure of a PAS histidine kinase from *Thermotoga maritima* (ThkA) was determined in complex with its response regulator (TrrA) (*50*). In this structure, the PAS domains are more than 100 Å apart and do not interact with each other. However, the ThkA construct lacks ~400 N-terminal residues comprising predicted coiled-coil and GAF domains, which can greatly facilitate protein dimerization (*51, 52*). Additional experiments are necessary to determine whether this arrangement of PAS monomers is physiologically relevant or arises from the particular, shorter construct used.

Do C-terminal flanking regions also play a role in establishing the quaternary structure of PAS domains? Different orientations of *bj*FixLH monomers are observed where in one case (R32) the C-terminal flanking helices are ordered and in the second case (P1AB and P1CD) they are disordered. The C-terminal helices in the *R*32 *bj*FixLH dimer interact with the helices from neighboring monomers. Although this specific orientation of its helices is likely to be a crystallization artifact, it demonstrates that interactions involving C-terminal helices could affect PAS domain quaternary structure.

Additional properties such as the presence of PAS domain effector domains and the composition of the dimer interface residues are likely to constrain PAS monomer orientation. In many cases, PAS domains function as protein interaction modules (*53*). However, PAS domain oligomerization may also be dictated by the effector domain to which they are linked. For example, full-length *ec*DOS, containing phosphodiesterase and heme-PAS domains, results in *ec*DOS tetramerization, whereas the heme-PAS domains alone can form only dimers (*54*). We conclude that the plasticity of PAS monomers makes their rearrangement particularly sensitive to their context. Therefore, PAS domain quaternary structure could differ depending on whether the PAS domains are isolated or are part of a full-length protein.

Maintaining the proper orientation of PAS monomers in the presence and absence of a signal appears to be critical for PAS sensor protein function. A single point mutation in a PAS domain from the sensor histidine kinase KinA from *B. subtilis* dimer interface residue may disrupt a monomer orientation. This in turn can lead to functional defects (*49, 55*). Signal-induced changes in quaternary structure are also observed in the PAS domain of a sensor histidine kinase from *Vibrio harveyi*, LuxQ (*56*).

Dimer Interface. PAS domain dimers contain a conserved dimer interface that is comprised of five structurally homologous residues located throughout the β-sheet in the A_β, B_β, H_β, and I_β strands (Figure 3) which interact with the β-sheet or N-terminal helix of another PAS domain. The conservation of the interface is surprising given the low level of sequence identity of the residues that comprise it. In most cases, the PAS dimer interface is comprised of hydrophobic residues that interact with residues from the opposing monomer in a specific "knobs-in-holes" fashion. In these cases, monomer orientation is sterically constrained. Notably, more than one solution to the knobs-in-holes problem is possible, as observed for the two crystal forms of *bj*FixLH (*P*1 and *R*32). Charged residues have also been found at a PAS dimer interface and can establish quaternary structure via electrostatic interactions. A PAS heterodimer involving PAS-B monomers from the human hypoxia-inducible factor (HIF)-2α and the aryl hydrocarbon nuclear translocator (ARNT) appears to be formed in part via electrostatic interactions between dimer interface residues of opposing monomers (*57*).

Network analysis (*43*) of the PAS dimer interface reveals that the interface is continuous, based on a single surface patch, rather than modular, based on two or more discrete surface patches. Thus, a single module establishes monomer affinity and quaternary structure and prevents the retention of quaternary structure when residue(s) within that module are mutated (*43*). Indeed, mutating a single residue at the KinA PAS dimer interface leads to large changes (>10-fold) in monomer affinity (*55*). The effect of deleting the N-terminus on the quaternary structure of PAS domains (*9, 45, 46*) is consistent with the predictions made using network

analysis: Disrupting part of a module leads to changes in quaternary structure (*43*).

Crystal Lattice Effects Have a Minimal Impact on CO-Induced Conformational Changes in bjFixLH. Crystal lattice effects are important to consider when using crystallography to study static protein structures and signal-induced conformational changes. While we cannot entirely rule out the effect of crystal packing, lattice effects on CO-induced conformational changes in *bj*FixLH appear to be quantitatively minor. Recently, it was shown that CO recombination kinetics of *bj*FixLH are closely similar in the *R*32 crystal form compared to those in solution (*18, 44*). This demonstrates that *bj*FixLH can readily convert between deoxy and CO states in the crystal and that intermolecular forces in the lattice that may affect the free energy barrier between the deoxy and CO-bound states have at most a minor effect. We directly compare the nature of the CO-induced conformational changes in *bj*FixLH crystallized in different crystal forms (*P*1, *R*32, and *C*2). We observe similar CO-induced conformational changes in each crystal form, despite very different intermolecular interactions and constraints within the three forms. This provides additional evidence of minimal crystal lattice effects on the integrity of the CO-bound structure of *bj*FixLH.

Role of Quaternary Structural Changes in the Signaling Mechanism of PAS Sensor Proteins. Previous studies have invoked the β-sheet in the signaling mechanism of PAS sensor proteins (*42, 57, 58*). Cusanovich and colleagues suggest (*58*) that a signaling event initiated within a PAS domain is transmitted from the ligand binding site to the dimer interface via distortion of the β-sheet. Our results are consistent with this hypothesis. Many PAS sensor proteins, including FixL, exist and function as oligomers (*53, 54*). While it is not necessary that an oligomer undergo quaternary structural changes to sense and respond to a signaling event, the quaternary structure of proteins often mediates allosteric communication. Quaternary structural changes originating in PAS domains could propagate to the linker region between the PAS and effector domain and ultimately to the effector domain itself. Signal-induced quaternary structural changes accommodate the ability of PAS sensor domains to regulate a wide variety of effector domains, since in such a model PAS and effector domains are not required to interact with each other in a structure-specific manner.

ACKNOWLEDGMENT

We thank Dr. Xiaojing Yang and Dr. Vukica Srajer and the staff of the 14 BM-C beamline, BioCARS, and APS for their assistance during data collection and processing and microspectrophotometer measurements. We thank Dr. Andreas Möglich and other laboratory members for helpful discussions. We acknowledge Dr. Marie-Alda Gilles-Gonzalez for the *bj*FixLH plasmid.

REFERENCES

1. Taylor, B. L., and Zhulin, I. B. (1999) PAS domains: Internal sensors of oxygen, redox potential, and light. *Microbiol. Mol. Biol. Rev. 63*, 479–506.
2. Crosson, S., Rajagopal, S., and Moffat, K. (2003) The LOV domain family: Photoresponsive signaling modules coupled to diverse output domains. *Biochemistry 42*, 2–10.
3. Crosson, S., McGrath, P. T., Stephens, C., McAdams, H. H., and Shapiro, L. (2005) Conserved modular design of an oxygen sensory/signaling network with species-specific output. *Proc. Natl. Acad. Sci. U.S.A. 102*, 8018–8023.
4. Gilles-Gonzalez, M. A., and Gonzalez, G. (2005) Heme-based sensors: Defining characteristics, recent developments, and regulatory hypotheses. *J. Inorg. Biochem. 99*, 1–22.
5. Gilles-Gonzalez, M. A., and Gonzalez, G. (1993) Regulation of the kinase activity of heme protein FixL from the two-component system FixL/FixJ of *Rhizobium meliloti*. *J. Biol. Chem. 268*, 16293–16297.
6. Parkinson, J. S., and Kofoid, E. C. (1992) Communication modules in bacterial signaling proteins. *Annu. Rev. Genet. 26*, 71–112.
7. Fischer, H. M. (1994) Genetic regulation of nitrogen fixation in rhizobia. *Microbiol. Rev. 58*, 352–386.
8. Kurokawa, H., Lee, D. S., Watanabe, M., Sagami, I., Mikami, B., Raman, C. S., and Shimizu, T. (2004) A redox-controlled molecular switch revealed by the crystal structure of a bacterial heme PAS sensor. *J. Biol. Chem. 279*, 20186–20193.
9. Miyatake, H., Mukai, M., Park, S. Y., Adachi, S., Tamura, K., Nakamura, H., Nakamura, K., Tsuchiya, T., Iizuka, T., and Shiro, Y. (2000) Sensory mechanism of oxygen sensor FixL from *Rhizobium meliloti*: Crystallographic, mutagenesis and resonance Raman spectroscopic studies. *J. Mol. Biol. 301*, 415–431.
10. Key, J., and Moffat, K. (2005) Crystal Structures of Deoxy and CO-Bound BjFixLH Reveal Details of Ligand Recognition and Signaling. *Biochemistry 44*, 4627–4635.
11. Gong, W., Hao, B., Mansy, S. S., Gonzalez, G., Gilles-Gonzalez, M. A., and Chan, M. K. (1998) Structure of a biological oxygen sensor: A new mechanism for heme-driven signal transduction. *Proc. Natl. Acad. Sci. U.S.A. 95*, 15177–15182.
12. Hao, B., Isaza, C., Arndt, J., Soltis, M., and Chan, M. K. (2002) Structure-based mechanism of O2 sensing and ligand discrimination by the FixL heme domain of *Bradyrhizobium japonicum*. *Biochemistry 41*, 12952–12958.
13. Gong, W., Hao, B., and Chan, M. K. (2000) New mechanistic insights from structural studies of the oxygen-sensing domain of *Bradyrhizobium japonicum* FixL. *Biochemistry 39*, 3955–3962.
14. Gilles-Gonzalez, M. A., Ditta, G. S., and Helinski, D. R. (1991) A haemoprotein with kinase activity encoded by the oxygen sensor of *Rhizobium meliloti*. *Nature 350*, 170–172.
15. Monson, E. K., Ditta, G. S., and Helinski, D. R. (1995) The oxygen sensor protein, FixL, of *Rhizobium meliloti*. Role of histidine residues in heme binding, phosphorylation, and signal transduction. *J. Biol. Chem. 270*, 5243–5250.
16. Möglich, A., and Moffat, K. (2007) Structural basis for light-dependent signaling in the dimeric LOV domain of the photosensor YtvA. *J. Mol. Biol. 373*, 112–126.
17. Richards, F. M. (1977) Areas, volumes, packing and protein structure. *Annu. Rev. Biophys. Bioeng. 6*, 151–176.
18. Gilles-Gonzalez, M. A., Gonzalez, G., Perutz, M. F., Kiger, L., Marden, M. C., and Poyart, C. (1994) Heme-based sensors, exemplified by the kinase FixL, are a new class of heme protein with distinctive ligand binding and autoxidation. *Biochemistry 33*, 8067–8073.
19. Otwinowski, Z., and Minor, W. (1997) Processing of X-ray diffraction data collected in oscillation mode. *Methods Enzymol. 276*, 307–326.
20. Kissinger, C. R., Gehlhaar, D. K., and Fogel, D. B. (1999) Rapid automated molecular replacement by evolutionary search. *Acta Crystallogr. D55*, 484–491.
21. Brunger, A. T., Adams, P. D., Clore, G. M., DeLano, W. L., Gros, P., Grosse-Kunstleve, R. W., Jiang, J. S., Kuszewski, J., Nilges, M., Pannu, N. S., Read, R. J., Rice, L. M., Simonson, T., and Warren, G. L. (1998) Crystallography & NMR system: A new software suite for macromolecular structure determination. *Acta Crystallogr. D54*, 905–921.
22. Murshudov, G. N., Vagin, A. A., and Dodson, E. J. (1997) Refinement of macromolecular structures by the maximum-likelihood method. *Acta Crystallogr. D53*, 240–255.
23. McRee, D. E. (1999) XtalView/Xfit: A versatile program for manipulating atomic coordinates and electron density. *J. Struct. Biol. 125*, 156–165.
24. Emsley, P., and Cowtan, K. (2004) Coot: Model-building tools for molecular graphics. *Acta Crystallogr. D60*, 2126–2132.
25. Koradi, R., Billeter, M., and Wuthrich, K. (1996) MOLMOL: A program for display and analysis of macromolecular structures. *J. Mol. Graphics 14*, 51–55, 29−32.
26. DeLano, W. L. (2002) The PyMOL Molecular Graphics System, DeLano Scientific, San Carlos, CA.

27. Krissinel, E., and Henrick, K. (2007) Inference of macromolecular assemblies from crystalline state. *J. Mol. Biol. 372*, 774–797.
28. Collaborative Computational Project Number 4 (1994) The CCP4 suite: Programs for protein crystallography. *Acta Crystallogr. d50*, 760–763.
29. Sobolev, V., Sorokine, A., Prilusky, J., Abola, E. E., and Edelman, M. (1999) Automated analysis of interatomic contacts in proteins. *Bioinformatics 15*, 327–332.
30. Batagelj, V., and Mrvar, A. (1998) Pajek: Program for Large Network Analysis. *Connections 21*, 47–57.
31. Krissinel, E., and Henrick, K. (2004) Secondary-structure matching (SSM), a new tool for fast protein structure alignment in three dimenstions. *Acta Crystallogr. D60*, 2256–2268.
32. Baldwin, J., and Chothia, C. (1979) Haemoglobin: The structural changes related to ligand binding and its allosteric mechanism. *J. Mol. Biol. 129*, 175–220.
33. Cox, J. M. (1967) Mathematical methods used in the comparison of the quaternary structures. *J. Mol. Biol. 28*, 151–156.
34. Kavanaugh, J. S., Rogers, P. H., and Arnone, A. (2005) Crystallographic evidence for a new ensemble of ligand-induced allosteric transitions in hemoglobin: The T-to-T(high) quaternary transitions. *Biochemistry 44*, 6101–6121.
35. Woltring, H. J., Huiskes, R., de Lange, A., and Veldpaus, F. E. (1985) Finite centroid and helical axis estimation from noisy landmark measurements in the study of human joint kinematics. *J. Biomech. 18*, 379–389.
36. Kabsch, W. (1976) *Acta Crystallogr. A32*, 922–923.
37. Tuckerman, J. R., Gonzalez, G., Dioum, E. M., and Gilles-Gonzalez, M. A. (2002) Ligand and oxidation-state specific regulation of the heme-based oxygen sensor FixL from *Sinorhizobium meliloti*. *Biochemistry 41*, 6170–6177.
38. Eisenberg, D., and McLachlan, A. D. (1986) Solvation energy in protein folding and binding. *Nature 319*, 199–203.
39. Jones, S., and Thornton, J. M. (1996) Principles of protein-protein interactions. *Proc. Natl. Acad. Sci. U.S.A. 93*, 13–20.
40. Key, J., Hefti, M., Purcell, E. B., and Moffat, K. (2007) Structure of the redox sensor domain of *Azotobacter vinelandii* NifL at atomic resolution: Signaling, dimerization, and mechanism. *Biochemistry 46*, 3614–3623.
41. Fedorov, R., Schlichting, I., Hartmann, E., Domratcheva, T., Fuhrmann, M., and Hegemann, P. (2003) Crystal structures and molecular mechanism of a light-induced signaling switch: The Phot-LOV1 domain from *Chlamydomonas reinhardtii*. *Biophys. J. 84*, 2474–2482.
42. Erbel, P. J., Card, P. B., Karakuzu, O., Bruick, R. K., and Gardner, K. H. (2003) Structural basis for PAS domain heterodimerization in the basic helix-loop-helix-PAS transcription factor hypoxia-inducible factor. *Proc. Natl. Acad. Sci. U.S.A. 100*, 15504–15509.
43. Reichmann, D., Rahat, O., Albeck, S., Meged, R., Dym, O., and Schreiber, G. (2005) The modular architecture of protein-protein binding interfaces. *Proc. Natl. Acad. Sci. U.S.A. 102*, 57–62.
44. Key, J., Srajer, V., Pahl, R., and Moffat, K. (2007) Time-resolved crystallographic studies of the heme domain of the oxygen sensor FixL: Structural dynamics of ligand rebinding and their relation to signal transduction. *Biochemistry 46*, 4706–4715.
45. Park, H., Suquet, C., Satterlee, J. D., and Kang, C. (2004) Insights into signal transduction involving PAS domain oxygen-sensing heme proteins from the X-ray crystal structure of *Escherichia coli* Dos heme domain (Ec DosH). *Biochemistry 43*, 2738–2746.
46. Watts, K. J., Sommer, K., Fry, S. L., Johnson, M. S., and Taylor, B. L. (2006) Function of the N-terminal cap of the PAS domain in signaling by the aerotaxis receptor Aer. *J. Bacteriol. 188*, 2154–2162.
47. Zoltowski, B. D., and Crane, B. R. (2008) Light Activation of the LOV Protein Vivid Generates a Rapidly Exchanging Dimer. *Biochemistry 47*, 7012–7019.
48. Ma, X., Sayed, N., Baskaran, P., Beuve, A., and van den Akker, F. (2008) PAS-mediated Dimerization of Soluble Guanylyl Cyclase Revealed by Signal Transduction Histidine Kinase Domain Crystal Structure. *J. Biol. Chem. 283*, 1167–1178.
49. Gomelsky, M., Horne, I. M., Lee, H. J., Pemberton, J. M., McEwan, A. G., and Kaplan, S. (2000) Domain structure, oligomeric state, and mutational analysis of PpsR, the *Rhodobacter sphaeroides* repressor of photosystem gene expression. *J. Bacteriol. 182*, 2253–2261.
50. Yamada, S., Akiyama, S., Sugimoto, H., Kumita, H., Ito, K., Fujisawa, T., Nakamura, H., and Shiro, Y. (2006) The signaling pathway in histidine kinase and the response regulator complex revealed by X-ray crystallography and solution scattering. *J. Mol. Biol. 362*, 123–139.
51. Martinez, S. E., Wu, A. Y., Glavas, N. A., Tang, X. B., Turley, S., Hol, W. G., and Beavo, J. A. (2002) The two GAF domains in phosphodiesterase 2A have distinct roles in dimerization and in cGMP binding. *Proc. Natl. Acad. Sci. U.S.A. 99*, 13260–13265.
52. Surette, M. G., and Stock, J. B. (1996) Role of α-helical coiled-coil interactions in receptor dimerization, signaling, and adaptation during bacterial chemotaxis. *J. Biol. Chem. 271*, 17966–17973.
53. Huang, Z. J., Edery, I., and Rosbash, M. (1993) PAS is a dimerization domain common to *Drosophila* period and several transcription factors. *Nature 364*, 259–262.
54. Yoshimura, T., Sagami, I., Sasakura, Y., and Shimizu, T. (2003) Relationships between heme incorporation, tetramer formation, and catalysis of a heme-regulated phosphodiesterase from *Escherichia coli*: A study of deletion and site-directed mutants. *J. Biol. Chem. 278*, 53105–53111.
55. Lee, J., Tomchick, D. R., Brautigam, C. A., Machius, M., Kort, R., Hellingwerf, K. J., and Gardner, K. H. (2008) Changes at the KinA PAS-A Dimerization Interface Influence Histidine Kinase Function. *Biochemistry 47*, 4051–4064.
56. Neiditch, M. B., Federle, M. J., Pompeani, A. J., Kelly, R. C., Swem, D. L., Jeffrey, P. D., Bassler, B. L., and Hughson, F. M. (2006) Ligand-induced asymmetry in histidine sensor kinase complex regulates quorum sensing. *Cell 126*, 1095–1108.
57. Card, P. B., Erbel, P. J., and Gardner, K. H. (2005) Structural basis of ARNT PAS-B dimerization: Use of a common β-sheet interface for hetero- and homodimerization. *J. Mol. Biol. 353*, 664–677.
58. Cusanovich, M. A., and Meyer, T. E. (2003) Photoactive yellow protein: A prototypic PAS domain sensory protein and development of a common signaling mechanism. *Biochemistry 42*, 4759–4770.
59. Holm, L., and Park, J. (2000) DaliLite workbench for protein structure comparison. *Bioinformatics 16*, 566–567.

BI801254C